

國立交通大學

電子工程學系電子研究所

碩士論文

應用於細胞圖形化和成長控制
之磁場平台設計與製造

Design and Fabrication of a Magnetic Microplatform
for Cell Patterning and Growth Controlling Application

研究生：黃睿婉

指導教授：鄭裕庭 教授

中華民國九十六年七月

應用於細胞圖形化和成長控制之磁場平台設計與製造

Design and Fabrication of a Magnetic Microplatform for Cell
Patterning and Growth Controlling Application

研究生：黃睿婉

Student : Jui-Wan Huang

指導教授：鄭裕庭

Advisor : Yu-Ting Cheng

國立交通大學
電子工程學系電子研究所
碩士論文

A Thesis

Submitted to Department of Electronics Engineering & Institute of Electronics

College of Electrical and Computer Engineering

National Chiao Tung University

in partial Fulfillment of the Requirements

for the Degree of

Master

in

Electronics Engineering

July 2007

Hsinchu, Taiwan, Republic of China

中華民國九十六年七月

應用於細胞圖形化和成長控制之磁場平台設計與製造

學生：黃睿婉

指導教授：鄭裕庭教授

國立交通大學電子工程學系暨電子研究所碩士班

摘 要

本論文主要是設計及製造一個可應用於細胞圖形化和成長控制之磁場平台。在矽基材上製造 5.5 圈的螺旋電感，通上 60Hz 的 AC 電流，可以產生 mT 等級的區域性磁場。磁場的強度及分布，還有可能的焦耳熱效應皆加以計算、模擬及量測。當加上熱電致冷片時，可以有效消除升溫，並將整個平台維持在攝氏 37 度。根據磁場可以增加細胞效應的研究[14-17]，加上細胞成長速率的增加和磁場強度成正比的關係，我們相信將細胞置於平台上時，電感的不同區域產生的不同的磁場強度會導致細胞有不同的成長效率，因而產生細胞圖形化的結果。

Design and Fabrication of a Magnetic Microplatform for Cell Patterning and Growth Controlling Application

student : Jui-Wan Huang

Advisors : Dr. Yu-Ting Cheng

Department of Electronics Engineering& Institute of Electronics
National Chiao Tung University

ABSTRACT

This thesis presents a magnetic microplatform design using localized magnetic field for cell patterning and growth controlling application. A 5.5-turns spiral inductor is designed and fabricated on a silicon substrate to generate the localized field with a mT-order magnitude while being loaded with 60Hz, $>0.1A$, AC current source. The magnetic field strength, field distribution on the spiral inductor is calculated, simulated using Ansoft Maxwell and measured. The possible joule heating effect is calculated, simulated using Ansoft-ePhysics and measured as well. In order to avoid temperature rise, a thermoelectric cooler is attached at the bottom of the device to control the whole platform at 37C. The magnetic field distribution of the inductor could make cell proliferation rate difference on cells different positions so cell patterning could be realized.

誌 謝

暫時要告別學生生涯，回想這麼多年的求學過程，一路上有親人朋友的真情相伴，師長們的不吝教導，所要感謝的人真的很多。

首先當然要感謝我的家人，從小到大，在物質上、精神上都是我最大支柱的父母，讓我不必為生活煩憂，也在我最脆弱的時候給予最有力的支持和關懷，使我得以更成熟堅強。還有跟我個性截然不同的老妹，有了手足之後生活也更有樂趣，也得到了一個優秀的服裝顧問。還有外公、外婆、姑姑、舅舅等等長輩們對我的疼愛、建言以及鼓勵。

除了家人之外，最應該感謝的人莫過於是指導教授鄭裕庭老師，兩年的研究生生活，老師的指導不僅讓我在學習如何做研究上有所進步，在其他方面老師也是一個很好的建議者。另外機械所徐文祥老師及其實驗室的學長和同學，尤其是黃家聖學長給我的協助。感謝中興大學資管系的蔡孟勳老師還有清大微機電所曾繁根老師的學生在細胞培養的相關問題上給予協助，感謝 Flying 幫我打線。

當然絕對不能忘記微系統整合實驗室的所有夥伴，子元還有胖子兩位勞苦功高的學長，抱歉問題都找你們解決，感謝你們的大力協助。上一屆的 Chando、思穎、小 B 還有 Jack，文駿、濬誠、還有下一屆的任楷、茄子、阿昌、Wesley 還有韋廷，大家都一起在研究室還有無塵室中度過了不短的時光。另外絕對不能忘記感謝的是 636 實驗室裡地位最高的助理筱筑，平常照顧我們大家，而且絕對不會在娛樂活動如吃飯、唱歌，出遊等缺席。雖然要離開 636 了，不過希望以後還是可以跟大家一起歡樂。

最後要感謝的，是這兩年來陪伴我的 Henry，督促我用功，傾聽我的牢騷，互相勉勵朝自己的目標邁進。如今我們都要邁入新的人生階段，要更加努力才行。

最後的最後，還是再一次的感謝所有的人，就是有你們的幫助，才有今日的我。

睿婉 2007/07/31

Contents

中文提要.....	i
Abstract	ii
誌謝.....	iii
Contents	iv
Figure Captions	v
Table Captions	vii
Chapter 1 Introduction	1
Chapter 2 Concept Design	4
2.1 Introduction	4
2.2 Dimensions of a Spiral Inductor.....	4
2.3 Determination of Magnetic Field	6
2.4 Determination of Temperature	11
Chapter 3 Fabrication Process.....	16
Chapter 4 Result and Discussion	19
Chapter 5 Conclusion and Future Work.....	24
5.1 Conclusion.....	24
5.2 Future Work	24
References	25

Figure Captions

Chapter 2

Figure 1. (a)Dimension of inductor. (b)Side view of air bridge. (c) Layout of inductors.	5
Figure 2. Calculation of the magnetic field at P_k on turn k due to current I flowing through an external turn j	7
Figure 3. Calculated magnetic field distribution. (a) The section chosen to demonstrate magnetic field distribution in (c) . (b) Magnetic field distribution at the inmost turn at 0.2A. (c) Magnetic field distribution on the chosen section at 0.2A.	9
Figure 4. Simulation result of magnetic field distribution at 0.2A. ...	10
Figure 5. Comparison of calculation and simulation results.	10
Figure 6. Temperature simulation result when input current is 0.2A. The hot spot is at the air bridge.	13
Figure 7. Comparison of calculation and simulation results.	15
Figure 8. Hot spot temperature under different input current under different environment.	15

Chapter 3

Figure 1. Fabrication process of a spiral inductor.	16
Figure 2. Device Setup.	18
Figure 3. Experimental Setup.....	18

Chapter 4

Figure 1. Comparison results for simulation and measurement.	20
---	----

Figure 2. Decay trend of measurement and 0.25mm from calculation.	20
Figure 3. Temperature versus time.....	22
Figure 4. Comparison the results from simulation and measurement from 0.1A~0.3A.	22

Table Captions

Chapter 1

Table 1. The introduction of some cell patterning approaches.	3
--	---

Chapter 2

Table 1. Values of properties used for temperature calculation.	12
--	----

Chapter 4

Table 1. AC magnetic field strength.	16
---	----

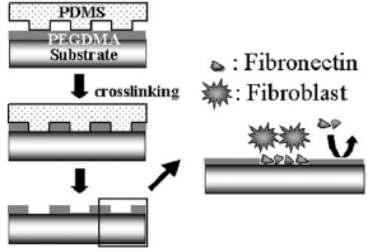
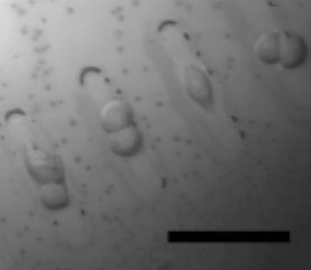
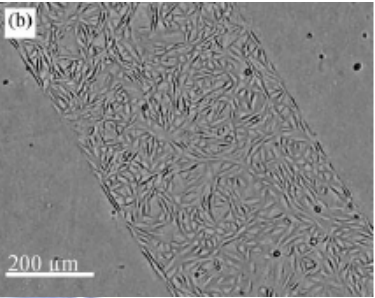
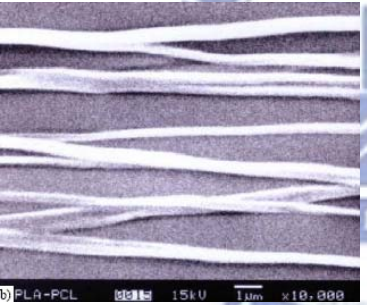
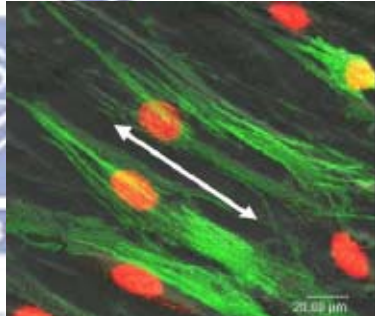
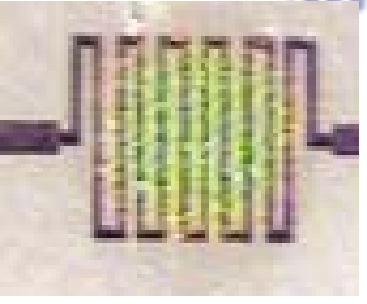
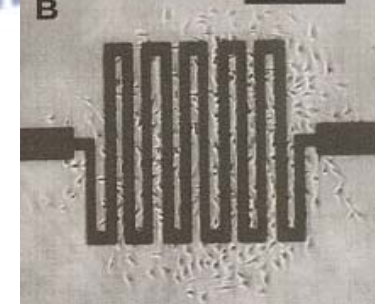
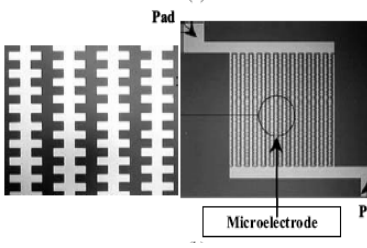
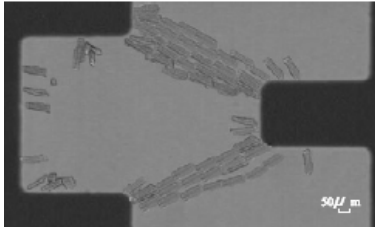
Chapter 1 Introduction

The loss or failure of an organ or tissue caused by diseases, accidents or aging is a great threat to human health. The major goal of tissue engineering is to provide therapies to repair or replace parts or whole damaged organs or tissue using artificial tissues. Functional tissues require cells to be placed at precise positions with precise orientations therefore cell patterning is the crucial step to fabricate artificial tissues. Table 1-1 introduces some cell patterning approaches. Nowadays, cellular patterns can be constructed using various lithographic methods such as soft lithography [1,2], laser-directed cell-writing [3], and inkjet printing [4]. Another widely studied approach is using scaffolds to induce the formation of new functional tissue from the originally dissociated mass of cells. Because of the 3-D morphology characteristic, scaffold can define and guide the formation of new tissues with appropriate function [5]. It is potential to be applied to the repair of various tissues such as smooth muscle [5], bone [6,7], cartilage [6,8,9], skin [10], and blood vessels [11]. In addition to the aforementioned conventional methods, some research groups have provided unique ideas such as adding thermal or electrical field to realize cell patterning. For example, Cheng et al. [12] controlled the polymer property to do cell patterning by modulating temperature of the polymer using a microheater array. Yang et al. [13] successfully constructed a cardiac myocyte tissue-like structure using combined dielectrophoresis and electro-orientation methods. In this thesis, a novel approach for cell patterning is proposed based on the modulation of cell growth rate under localized magnetic field. Previously, researches have shown that cells' behavior was altered under magnetic field exposure. For instance, Heredia-Rojas et al. [14] reported that 60Hz magnetic field has lead to

stimulation of lymphocytes proliferation. Katsir et al.[15] showed increase in proliferation of chicken embryo fibroblasts after 24hr exposure under 60Hz, 0.7mT magnetic field. De Mattei et al.[16] reported that cell proliferation increase of human normal osteoblasts is observed after 6hr or longer exposure by pulsed electromagnetic field. Kwee and Velizarov [17] found a linear correlation between field strength and exposure time needed to reach maximum proliferation rate of transformed human epithelial amnion cells.

In the aforementioned researches, a uniform magnetic field was generally applied to observe possible effects on the cells' behavior. Thus, in this thesis, a localized magnetic field will be introduced by designated on-chip spiral inductors which can easily concentrate magnetic field in themselves and modulate the field strength by different electrical current inputs. Cells at different regions are exposed under different magnetic field strengths. As a result, cell patterning could be achieved due to different proliferation rate at different locations. The magnetic microplatform design and fabrication including magnetic field and temperature control and the fabrication of on-chip spiral inductor are described as follows.

Table1-1. The introduction of some cell patterning approaches.

Approaches	Setup	Results	Reference
Soft-lithography	 <p>PDMS PEODMA Substrate</p> <p>↓ crosslinking</p> <p>▲ : Fibronectin ★ : Fibroblast</p>		[1]
Inkjet Printing	Modified commercial printer with different solutions	 <p>(b)</p> <p>200 μm</p>	[4]
Scaffold	 <p>b) PLA-PCL 15kV 1.0μm x18,000</p>	 <p>20.00 μm</p>	[11]
Microheater-controlled thermo-responsive plasma films		 <p>B</p>	[12]
Microfluidic dielectrophoresis chip	 <p>Pad</p> <p>Microelectrode</p> <p>Pad</p>	 <p>50 μm</p>	[13]

Chapter 2 Concept Design

2.1 Introduction

The localized magnetic field is generated by spiral inductors. A spiral inductor has several advantages: (1) It is compatible to CMOS post-process. (2) It can be miniaturized to fit dimensions of cells. (3) It can concentrate magnetic field efficiently. (4) The distribution of magnetic field is able to make cells at different region of inductor be exposed under different strength. (5) The magnetic field strength is proportional to input current thus it can be modulated by input current. The frequency we choose is 60Hz, the same as it of the household power supply. Many researches [14, 18-20] have done at this frequency due to the interest in biological effects between magnetic field generated by household power with organisms. We also use this frequency in order to compare our result with others. From previous study [21], field strength larger than 1.0mT can induce significant proliferation of fibroblasts therefore our device should be able to generate magnetic field larger than 1.0mT.

2.2 Dimensions of a Spiral Inductor

The line width of a spiral inductor is chosen to be 75 μ m, the same order of dimensions of cells but larger therefore cells can experience different field strength on each turn. That is, the magnetic field distribution is apparent to cells. The spacing is 25 μ m and the thickness is 5 μ m. The outmost diameter is 1500 μ m.

The air bridge is 10 μ m above the coil and its thickness is also 5 μ m. The exposure system consists of 12 spiral inductors equally divided into 3 groups. The spacing between each inductor in the same group and that between each group is 2.5mm and 13mm, respectively. Figure 2-1 shows the dimensions of the inductor and the layout of the whole platform. In order to make sure that cells' response is due to magnetic field exposure, not all inductors in the platform are can be turned on. Only one inductor in the first group can be turned on. All inductors are not functional in the second groups. In the third group, all inductors are connected to both pads and are able to produce magnetic field.

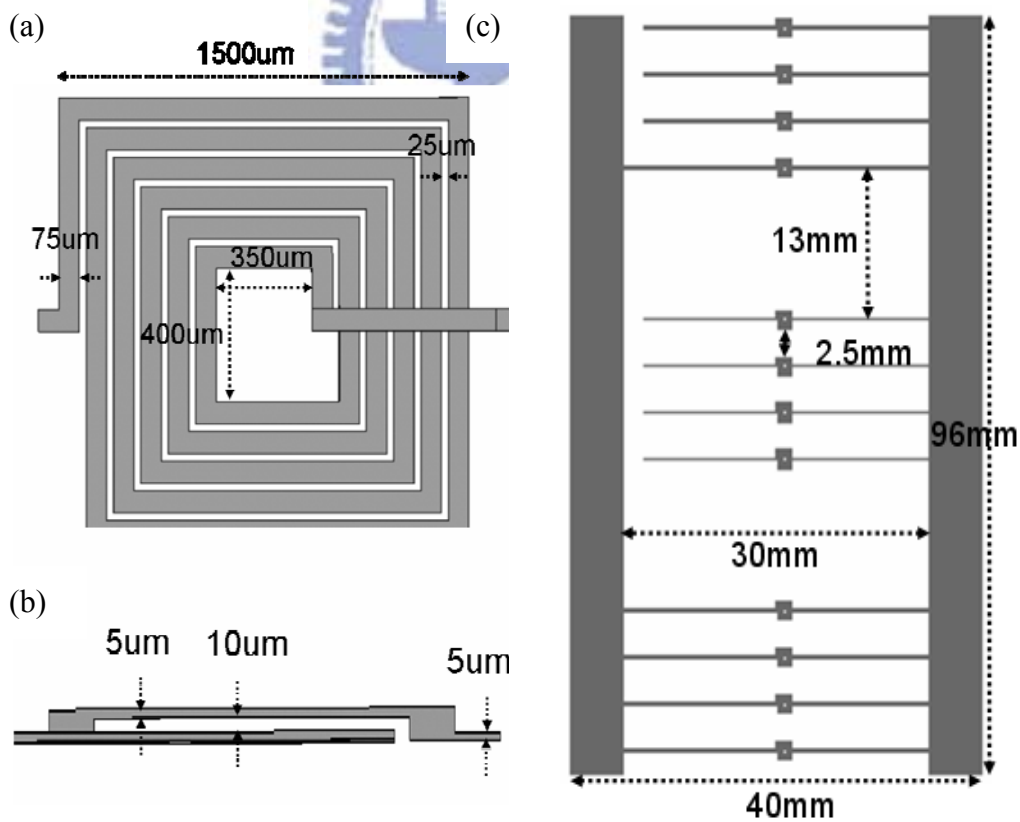


Figure 2-1. (a) Dimensions of inductor. (b) Side view of air bridge. (c)Layout of inductors.

2.3 Determination of Magnetic Field

The magnitude and distribution of the localized magnetic field are evaluated using the analytical model proposed by Ibrahim and Kuhn [22]. Although the model was developed for the prediction of DC magnetic field the frequency we will use is 60Hz, which is low enough to be approximated using model for DC.

In this model, the spiral is treated as a collection of segments, partitioned as those inside the turn of interest, those outside the turn, and those for the turn itself. A closed-form of magnetic field at any point inside the spiral is derived based on the sum of superpositioned fields from each segment [22]. Fig 2-2 indicates parameters used in calculating magnetic field. While turn j is outside of turn k , flux density on a point P_k on turn k induced by turn j are:

$$\begin{aligned}
 B_{j1} &= \frac{\mu_0 I}{4\pi c_1} (\cos \theta_{12} - \cos \theta_{11}) \\
 B_{j2} &= \frac{\mu_0 I}{4\pi c_2} (\cos \theta_{22} - \cos \theta_{21}) \\
 B_{j3} &= \frac{\mu_0 I}{4\pi c_3} (\cos \theta_{32} - \cos \theta_{31}) \\
 B_{j4} &= \frac{\mu_0 I}{4\pi c_4} (\cos \theta_{42} - \cos \theta_{41})
 \end{aligned} \tag{1}$$

where constant c 's are given by

$$\begin{aligned}
 c_1 &= (s + w)(j - k) \\
 c_2 &= (s + w)(j - k) + \left(\frac{D_k}{2} + X_0 \right) \\
 c_3 &= D_j - c_1 \\
 c_4 &= (s + w)(j - k) + \left(\frac{D_k}{2} - X_0 \right)
 \end{aligned}$$

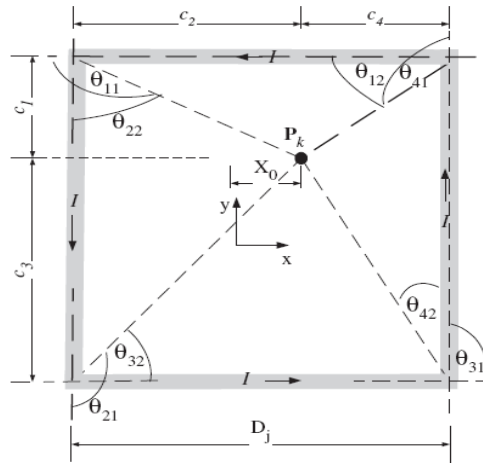


Figure 2-2. Calculation of the magnetic field at P_k on turn k due to current I flowing through an external turn j . [22]

Where s represents the spacing between each turn, w represents the width of the coil, $D_j \cdot D_k$ are the side length of turn j and k , and x_0 is the distance between P_k and the y -axis. The angles are calculated as follows:

$$\begin{aligned}
 \cos \theta_{11} &= -\frac{c_2}{\sqrt{c_1^2 + c_2^2}} \\
 \cos \theta_{12} &= \frac{c_4}{\sqrt{c_1^2 + c_4^2}} \\
 \cos \theta_{21} &= -\frac{c_3}{\sqrt{c_2^2 + c_3^2}} \\
 \cos \theta_{22} &= \frac{c_1}{\sqrt{c_1^2 + c_2^2}} \\
 \cos \theta_{31} &= -\frac{c_4}{\sqrt{c_3^2 + c_4^2}} \\
 \cos \theta_{32} &= \frac{c_2}{\sqrt{c_2^2 + c_3^2}} \\
 \cos \theta_{41} &= -\frac{c_1}{\sqrt{c_1^2 + c_4^2}} \\
 \cos \theta_{42} &= \frac{c_3}{\sqrt{c_3^2 + c_4^2}}
 \end{aligned} \tag{2}$$

And the summation of the magnetic field at point P_k is

$$B_j^k = -B_{j1} - B_{j2} - B_{j3} - B_{j4} \quad (3)$$

Magnetic flux densities induced by turns inside turn k are calculated using the same approach with some parameters modified. Magnetic field generated by the same turn is neglected in counting it in z -direction since only the y components exist. The magnetic field distribution was obtained by writing a MATLAB code.

From the calculation, the characteristics of magnetic field distribution are found. Magnetic field is larger at inner turns and turn corners. Extreme values occur at inner edges and outer edges of each turn. The maximum value occurs at the inner edge of the inmost turn and it decays towards the center of the inductor. Fig. 2-3 shows the magnetic field distribution on a segment of the inmost turn and a section. We also use electromagnetic simulation software Ansoft-Maxwell to calculate magnetic field distribution. Fig. 2-4 shows the simulation result of magnetic field distribution on a spiral inductor at 0.2A. Fig. 2-5 shows the comparison of magnetic field strength between the Ansoft simulation and the analytical calculation. The field induced by the analytical model with DC current input is close to the value calculated by the simulator. It indicates that our assumption for field strength calculation using the analytical model is reasonable. It is noted that the magnetic field calculated by the simulator is slightly larger than that derived by the model. The underestimation is mainly due to only 5 closed loops are used for the calculation for simplicity while in reality it has 5.5 turns.

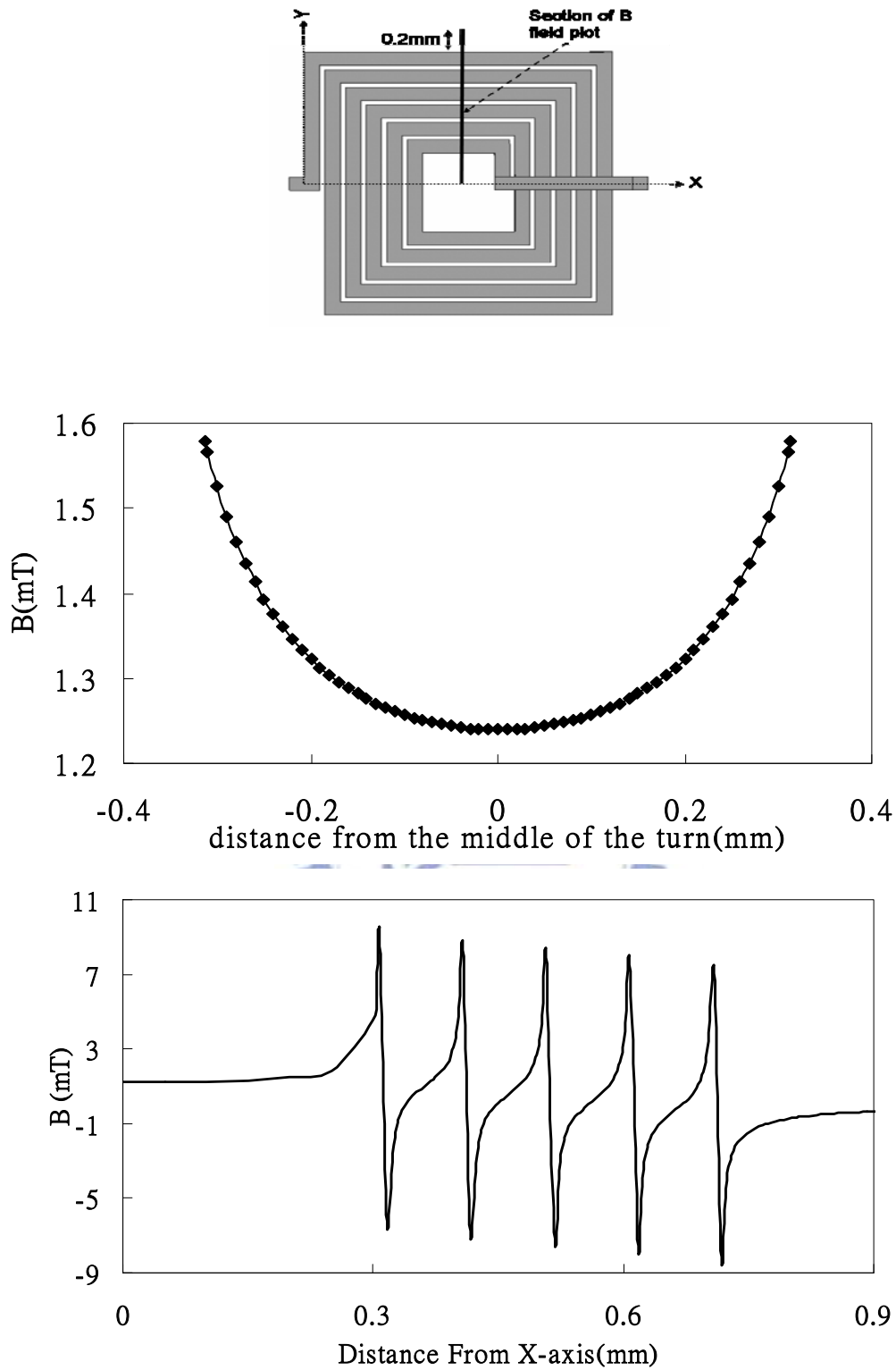


Figure 2-3. Calculated magnetic field distribution. (a)The section chosen to demonstrate magnetic field distribution in (c). (b) Magnetic field distribution at the innermost turn at 0.2A. (c) Magnetic field distribution on the chosen section at 0.2A.

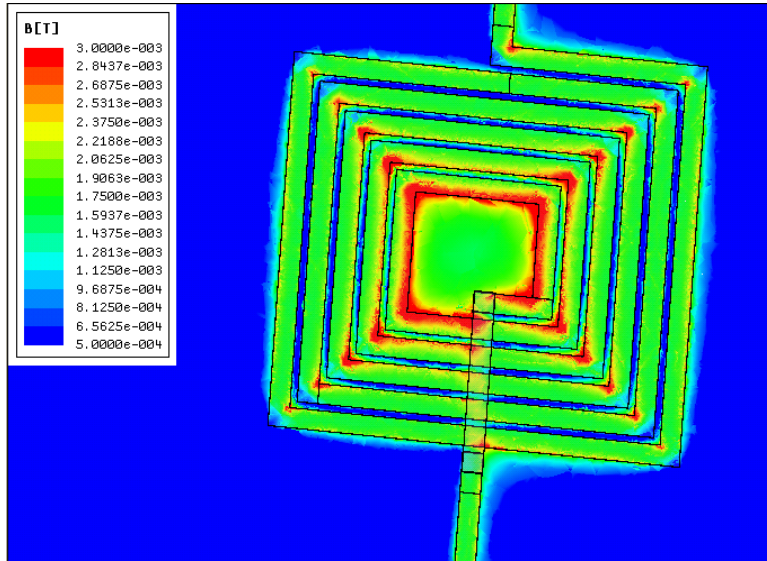


Figure 2-4. Simulation result of magnetic field distribution at 0.2A.

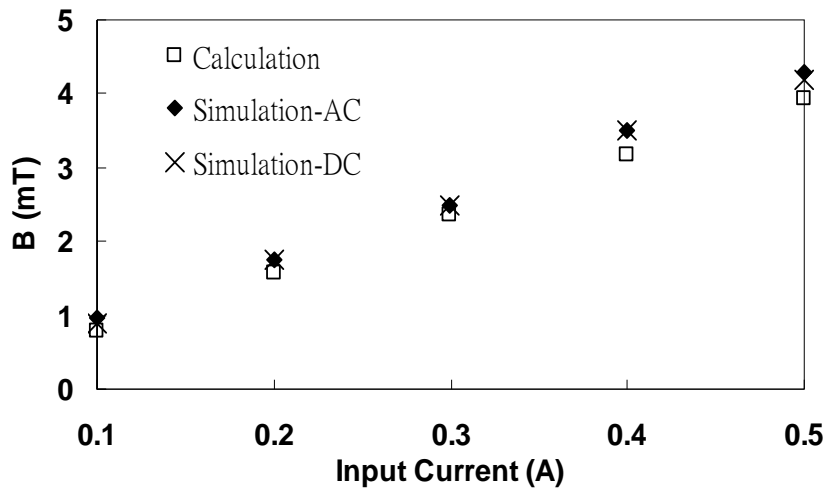


Figure 2-5. Comparison of calculation and simulation results.

2.4 Determination of Temperature

Cell proliferation rate is very sensitive to environmental temperature. Many researches [14-20] related to cell culture, incubation systems have kept the temperature precisely at 37°C, which has been found to be the most suitable temperature for mammalian cells to survive. As a result, when we applied the device on cells, the ambient temperature must be kept at 37°C as well. Thus, the temperature control on the spiral inductor is very critical. In addition, according to the previous study [21], about 1mT magnetic field is required to have significant increase in cell proliferation rate. Thus, based on the analysis, at least 0.1A input current should be chosen for realize our goal and the joule heating effect resulted by such a current input should be considered in the platform design.

In the platform design, the temperature rise of inductors is evaluated using the model proposed by Lin et al. [23]. The model is used to count temperature rise on a microheater with a current input. Variables ε and T_{ref} are defined as follows:

$$\varepsilon = \frac{k_{\text{si}} F}{k_{\text{cu}} z_{\text{cu}} z_{\text{si}}} - \frac{J^2 \rho_{\text{cu}} \xi_{\text{cu}}}{k_{\text{cu}}} \quad (4)$$
$$T_{\text{ref}} = T_{\infty} + \frac{J^2 \rho_{\text{cu}}}{k_{\text{cu}} \varepsilon}$$

where k , z , J , ρ , and ξ represents thermal conductivity, thickness, current density, and temperature coefficient of resistivity. Subscript cu and si represents copper and silicon. Values of these properties are listed in Table 2-1.

Table 2-1. Values of Properties Used for Temperature Calculation

k_{si}	k_{cu}	z_{si}	z_{cu}	ρ_{cu}	ξ_{cu}
148	401	5.25E-4	5E-6	1.6E-8	3.93E-4
W/m°C	W/m°C	m	m	Ωm	1/°C

The maximum steady state occurs at the middle of a turn:

$$T_{\max} = T_{\text{ref}} + \frac{(T_{\text{ref}} - T_{\infty})}{\cosh(\sqrt{\varepsilon} L/2)} \quad (5)$$

Formulas are modified to fit our situation. Firstly, the line width of designed spiral inductor is much larger than that of microheater [23], therefore the shape factor, F , is reduced to 1. Secondly, the temperature of whole silicon substrate in this model is set at ambient temperature. Only the heating zone is confined within the isolation layer underneath the microheater. In comparison with our microplatform, a silicon substrate with spiral inductor on top of itself mounted on a PCB, the bottom temperature of the silicon substrate should be set at the temperature we measured right at the back side of PCB because the poor thermal conductivity of PCB that would lead to temperature rise at the bottom of the silicon substrate. Finally, we ignore silicon nitride isolation layer due to its thickness (1000Å) is relatively small by comparing with that of silicon substrate (550µm).

Meanwhile, the temperature distribution of the spiral inductor is simulated using Ansoft-ePhysics. Fig. 2-6 shows the simulation result of the spiral inductor with 0.2A current input. The hot spot is at the air bridge of the inductor due to the poor thermal conductivity of the air underneath the bridge. Although the

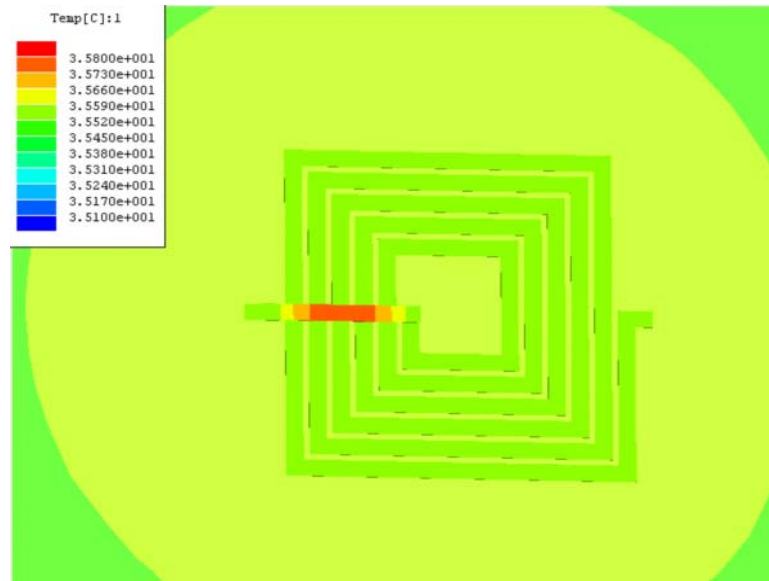


Figure 2-6. Temperature Simulation Result when input current is 0.2A. The hot spot is at the air bridge.

temperature is slightly lower in the rest part of the inductor, the temperature of the whole inductor as well as that of surrounding air are still risen above the ambient temperature. While the ambient temperature is 25°C and the whole device is put in air, the temperature rise of the spiral inductor with the input current of 0.1, 0.2, and 0.3A are 1.58°C 、 6.16°C 、 13.8°C respectively. The result indicates that the temperature of whole device increases dramatically with the increase of electric current. When input current is larger than 0.4A, the temperature rise is high enough to damage the device and cause fatal effect to cells. In addition, in comparison with the calculation from the aforementioned microheater model as shown in Fig. 2-7. The temperature rise calculated by Ansoft simulator is slightly larger. The reason is that the spiral inductor should be treated as a group of microheaters arranged side by side therefore the temperature should be higher than the calculation result for a single resistor.

In reality, the surrounding environment of the platform is changed to water instead of air in order to make the whole simulation closer to the experimental

setup for cell culturing. Fig. 2-8 shows the hot spot temperature under different current input. It is obvious to see the reduction of the temperature rise because of the additional heat capacity by the introduction of water. Nevertheless, since the whole system including our microplatform will be kept at 37°C as mentioned, the boundary temperature should be set at 37°C instead of 25°C. Both from the aforementioned model calculation and simulation, the temperature rise of platform is inevitable and the interface between the inductor and incubated cells will be higher than 37°C while the inductor is loaded with a current input. Especially, when the input current increases up to 0.5A, temperature rise about 7°C will cause heat-induced cell death. Thus, a thermoelectric cooler is used to keep the bottom of the device with a steady and lower temperature to keep the device at 37°C. For example, when applying 0.2A, without the cooler, the highest temperature is 31.16°C. If a cooler is attached to the bottom of the device keeping the bottom of the device at 1°C lower than ambient temperature, the hot spot temperature will be lower to 25.017°C.

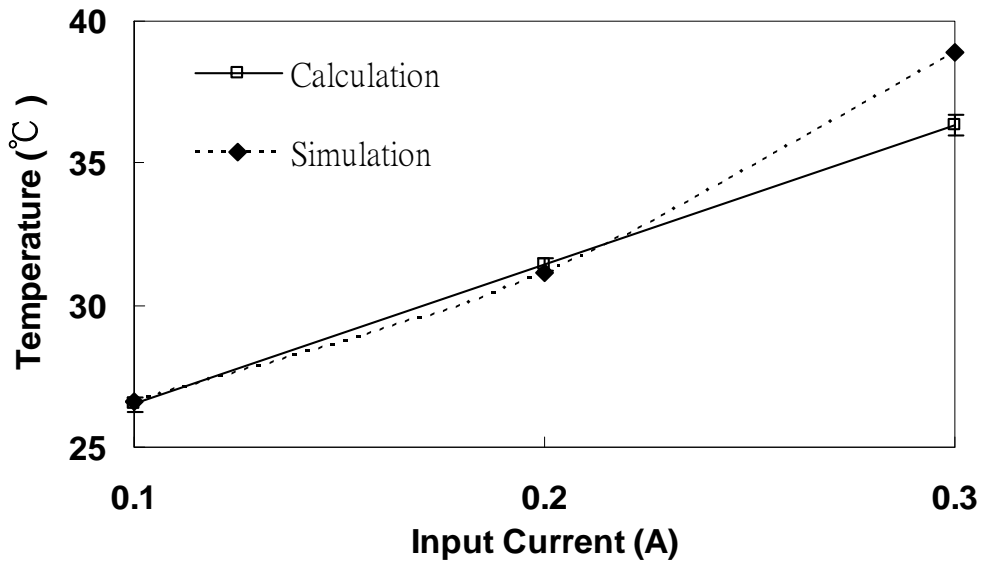


Figure 2-7. Comparison of calculation and simulation results.

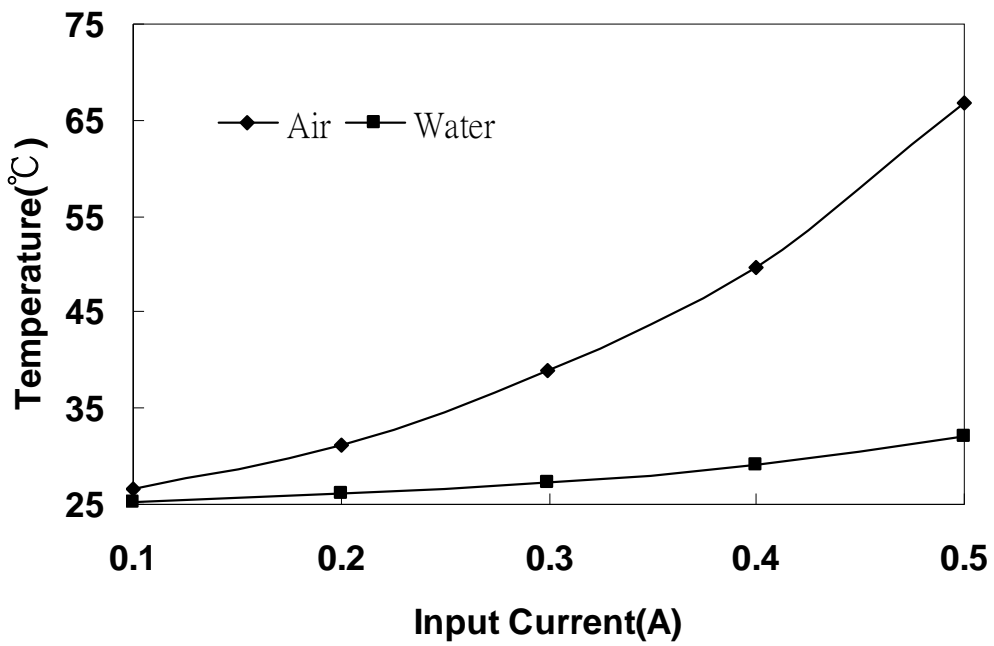


Figure 2-8. Hot spot temperature under different input current under different environment.

Chapter 3 Fabrication Process

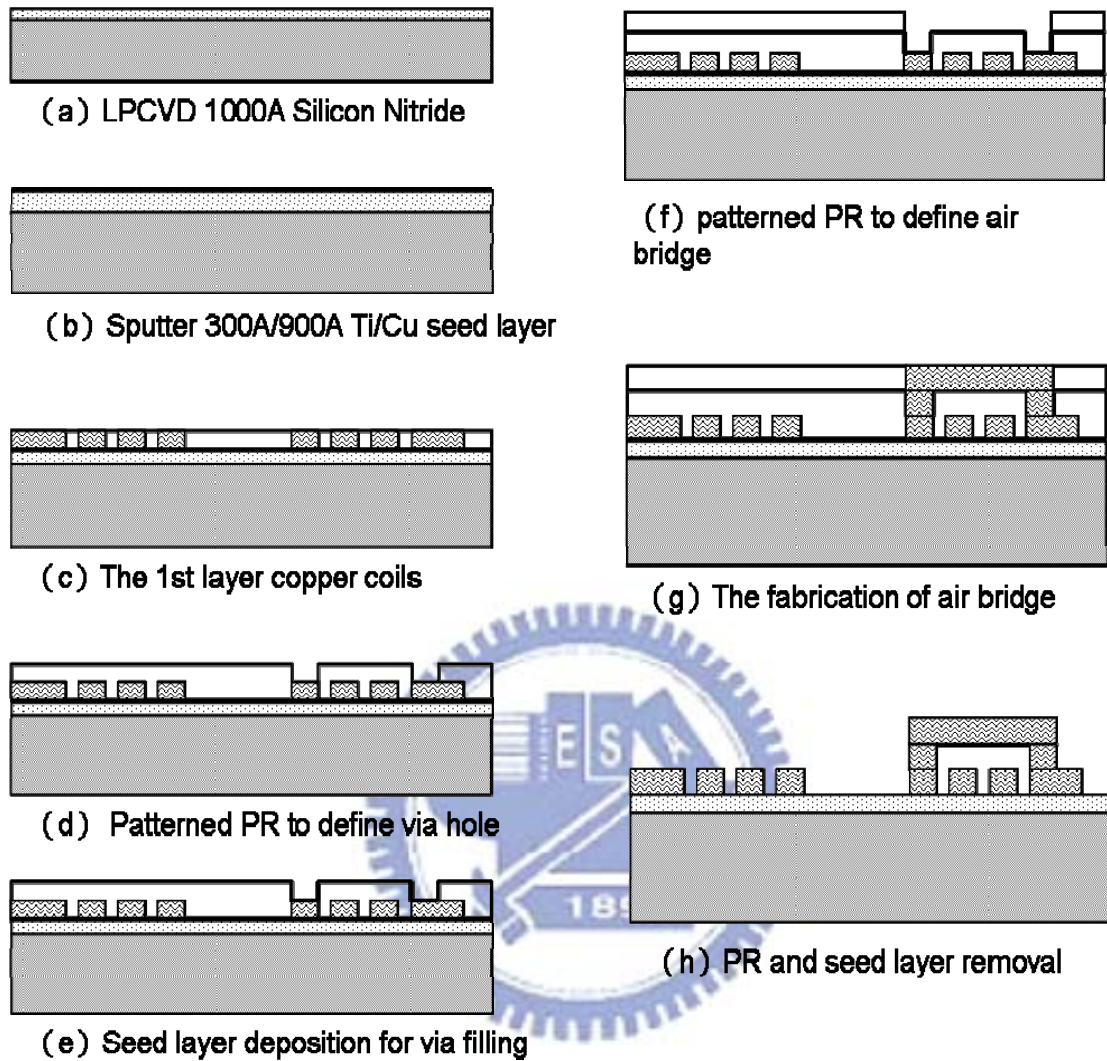


Figure 3-1. Fabrication process of a spiral inductor.

The inductors are fabricated starting with 1000A LPCVD nitride on silicon substrate and then Ti/Cu (300A /900A) adhesion/seed layer is sputtered onto isolation layer shown in figure 3-1(a). Figure 3-1(b) shows that a patterned $7\mu\text{m}$ thick AZ 4620 photo-resist to define the region of the coil part of the spiral inductor then coils are fabricated by copper electroplating. After plated the first layer of copper, a $10\mu\text{m}$ AZ4620 layer is spin-coated, patterned to define the via hole in figure 3-1(c), and sputtered with another 100nm copper seed layer in

figure 3-1(d) for the air-bridge copper via filling. Figure 3-1(e) illustrates that, after the seed layer of the via filling, another 10 μm AZ4620 is spun onto the plated structure, patterned to define the air-bridge beam, and plated with 5 μm copper to form the air bridge as showed in figure 3-1(f). Finally, the fabrication of the spiral inductor is done after lift off the underneath copper seed layer and chemically etch away the first seed/adhesion layer using CR-7T and BOE as shown in figure 3-1(g).

After completing the fabrication of spiral inductors, the chip is bonded to a printed circuit board (PCB) in order to connect to power source. Conducting paths between chip and PCB are gold wires. In order to confine cells and culture solutions in the inductor region, quartz tubes are used to bond with chip using silica gel to form a cell container-like structure. The device setup is shown in Fig. 3-2.

After the device is fabricated, a biocompatible layer is coated on the surface of the device in order to enhance the adhesion of cells. The material used for coating can be collagen, fibronectine, or poly-L-lysine, based on cell type. Then the device is immersed in the alcohol for 30 min to do sterilization. After sterilization, it can be used for cell culture. The experimental setup is shown in Fig. 3-3.

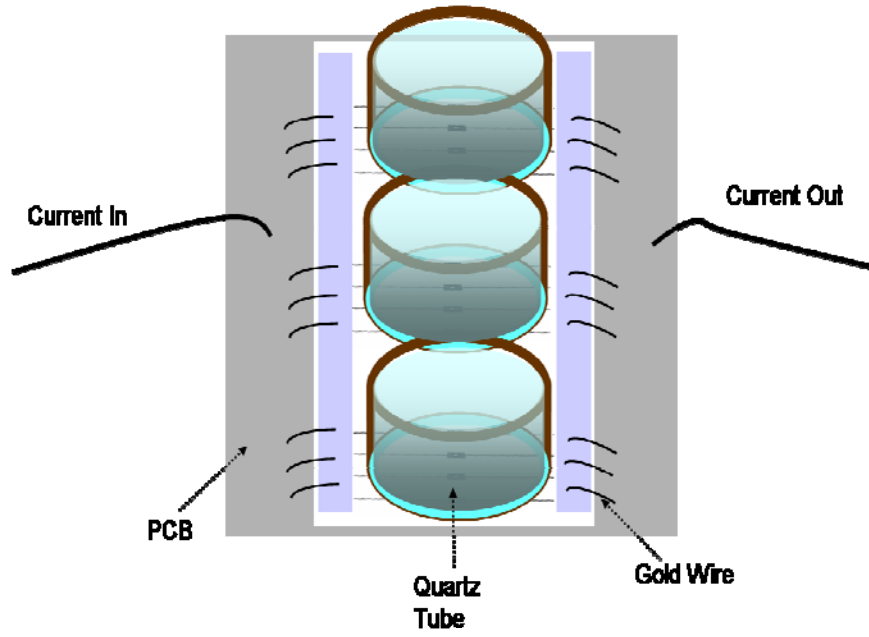


Figure 3-2. Device Setup

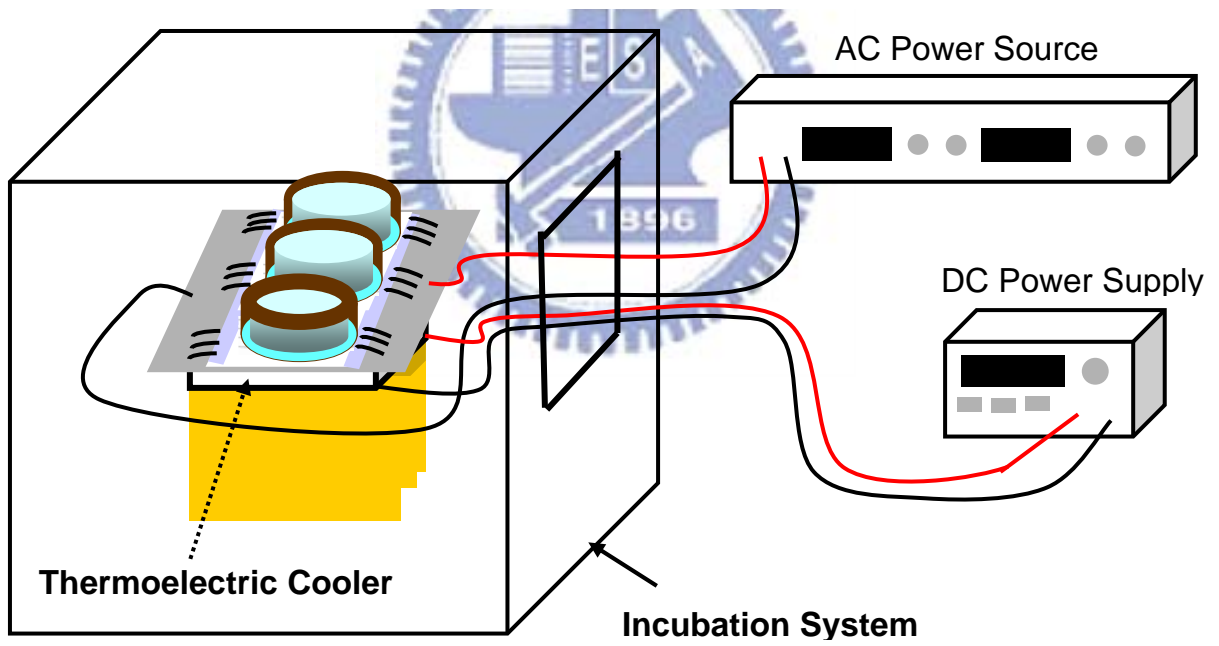


Figure 3-3. Experimental Setup

Chapter 4 Result and Discussion

The magnetic field of each inductor has been measured using a Gaussmeter (TM601, Kanetec, Japan) with a transverse probe. Measurement is done by applying both DC and AC current. Figure 4-1 compares the results for simulation and measurement. It is clear to see that magnetic fields generated by DC and AC current have no much difference. AC measured value is only 24% and 22% of calculated and simulation values. The possible reasons is that measurement is the most accurate when the probe perfectly contacts the device. The air bridge part may make the probe not contact the device and the reading would be smaller than real value due to a distance between the probe and the device. Besides, the probe is held by hand therefore we cannot precisely control the distance between the probe and the device. In order to determine the distance, we placed pads with a known thickness which is 0.525mm next to the device to keep the probe at certain heights. Since measured values in DC and AC have no much difference, Biot-Savart law is applicable to evaluate AC magnetic field decay with height, then fit the decay trend with measurement ones. The original distance between the probe and the device is 0.25mm, Fig. 4-2 shows the decay trend from measurement and that of 0.25mm above the device. From Biot-Savart law, the magnetic field above the device of 0.25mm is 59% of that on the device. After modulating the measured values to eliminate the distance effect, they are still smaller than calculated and simulated values by 59% and 63%. The modulated values are also shown in Table 4-1. Table 4-1 shows the magnetic field strength obtained by calculation, AC simulation, and AC measurement. After eliminating the distance effect, the modified results still have great difference with simulation and calculation ones. Another possible

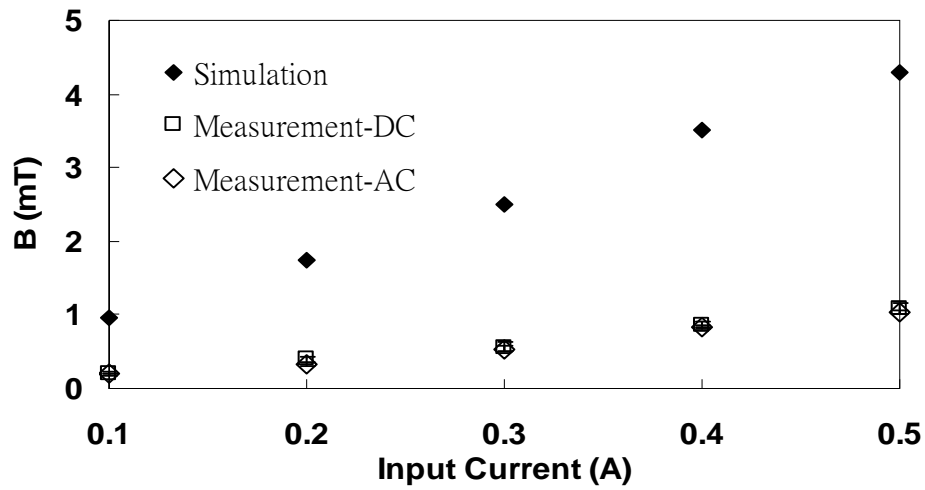


Figure 4-1. Comparison results from simulation and measurement.

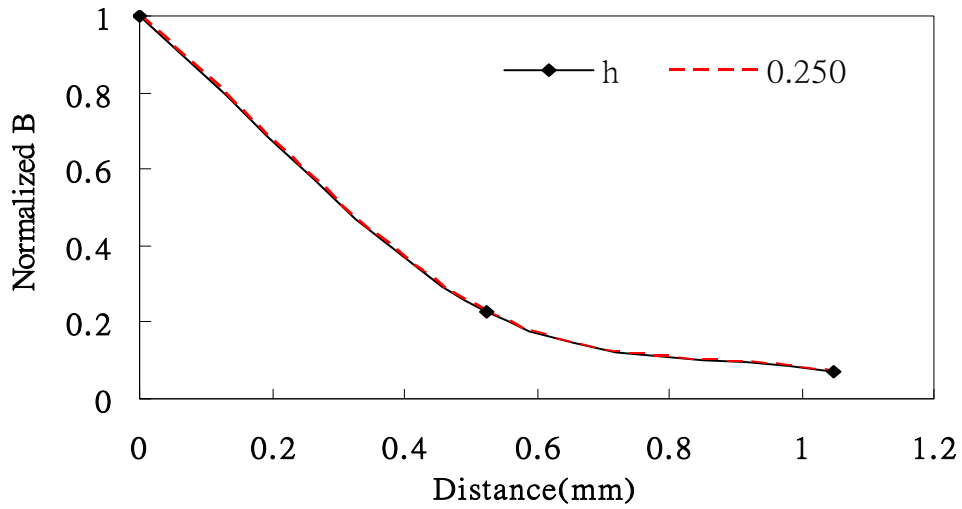


Figure 4-2. Decay trend of measurement and 0.25mm from calculation.

Table 4-1. AC Magnetic Field Strength

Magnetic Field(mT)	Input Current (A)				
	0.1	0.2	0.3	0.4	0.5
Simulation	0.96	1.75	2.5	3.5	4.3
Calculation	0.79	1.58	2.37	3.16	3.94
Measurement	0.190	0.326	0.540	0.834	1.034
Measurement-modified	0.324	0.556	0.921	1.423	1.764

reason is that the probe of the Gaussmeter measures magnetic field strength using the Hall Effect. It is usually used to measure uniform magnetic field. However, in our case the magnetic field is not uniform in its active area. the nominal diameter of the sensing area of the probe is $2\text{mm}\times 2\text{mm}$, which is even larger than the dimension of the inductor ($1.5\text{mm}\times 1.5\text{mm}$) therefore our measurement has its restrictions.

Measurement of temperature is done by using thermocouple. The measurement in air was done using thermocouple type K connected to a thermometer (YS-822R, YSC, Taiwan) . The thermocouple was attached the substrate at a fixed point. The temperature difference between the measure point and the hot spot is derived from simulation. The results of temperature over time were plotted in Figure 4-3, with temperature modified to it at the hot spot. The ambient temperature was 25°C when we did measurement. If temperature rose above 42°C , the measurement was terminated. The first reason is that the highest tolerable temperature of mammalian cells is 42°C . If the device is higher than this temperature, it will kill cells. Another reason is to avoid the device damaged by high temperature. It is clear from the figure that when applied current is above 0.4A , it rose above 42°C quickly. For currents under 0.3A , the highest temperatures are lower than 40°C , and it reaches steady state within 10 minutes with only small oscillation.

Fig. 4-4 compares the results from simulation and measurement from $0.1\text{A}\sim 0.3\text{A}$. The results have no much difference. Simulated values are slightly lower due to ideal parameters and perfect conduction. We apply a thermoelectric

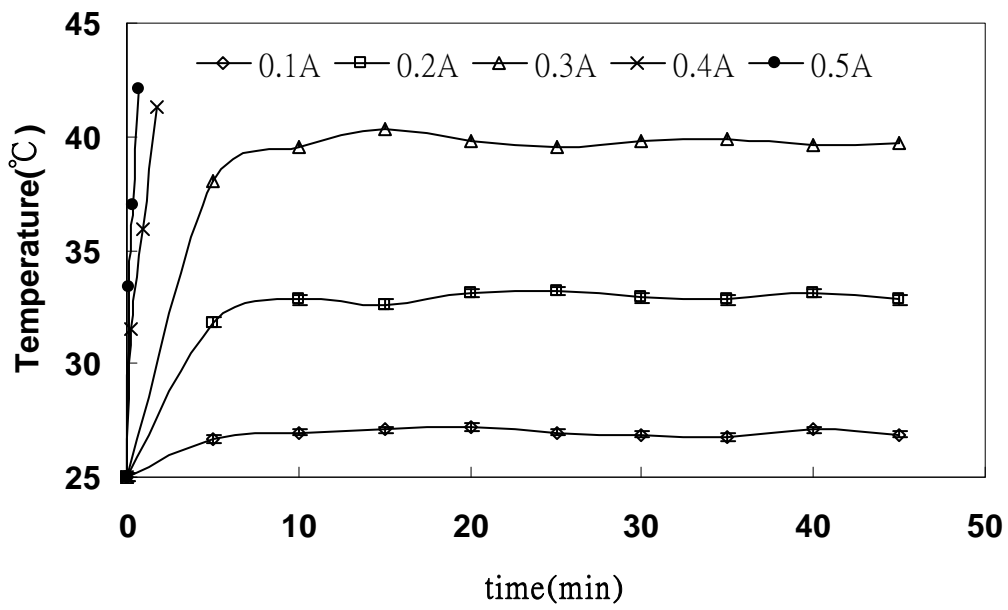


Figure 4-3. Temperature versus time

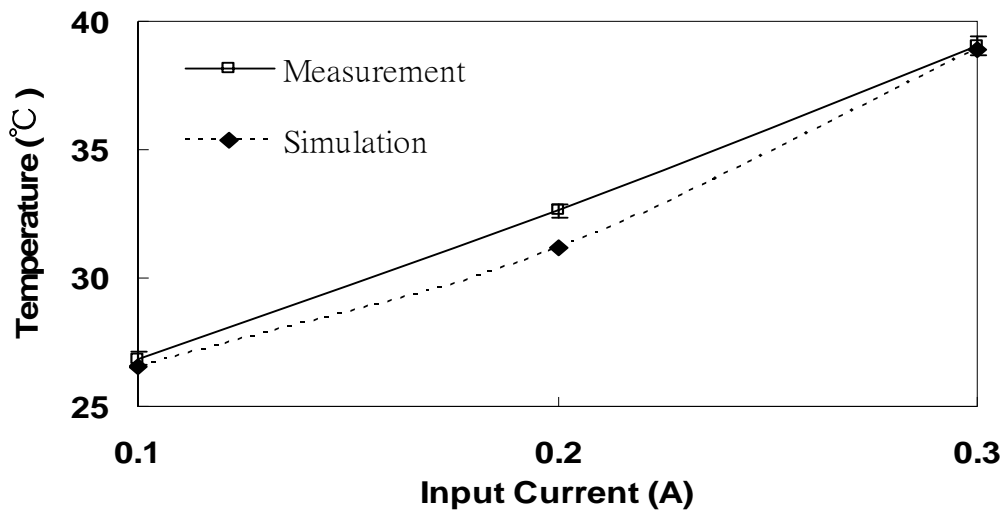
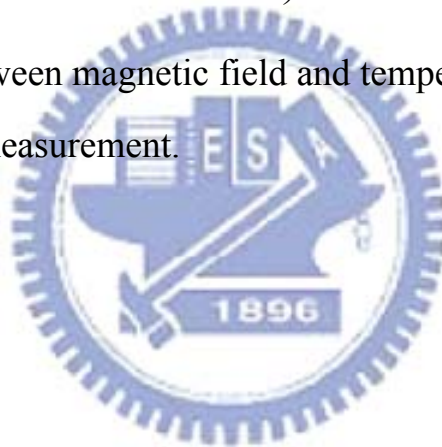


Figure 4-4. Comparison the results from simulation and measurement from 0.1A~0.3A.

cooler attached to the bottom of the device in order to keep the device from temperature rising. When input current is larger than 0.3A, the temperature rise is smaller when applied cooler, but it still cannot stop temperature rise when input current of cooler is 1A. Although the larger the input current of thermoelectric cooler, the better the cooling is, the input current also generates magnetic field, in order not to interfere the field generated by inductors, the input current of the cooler cannot be too large. When input current of an inductor is 0.2A, it has no temperature rise when input current of the cooler is 0.4A, and the DC magnetic field generated by the cooler is 0.1mT. Input total current of 1.0A (each inductor is 0.2A) is the most suitable value of an acceptable trade-off between magnetic field and temperature based on the results of the simulations and measurement.



Chapter 5 Conclusion and Future Work

5.1 Conclusion

The magnetic microplatform with spiral inductors has been successfully designed and fabricated. The magnetic and temperature field on the spiral inductor are calculated, simulated, and measured. Localized magnetic field of 1.75mT is generated by input current 0.2A. The magnetic field measurement result has apparent difference with simulation and calculation due to the dimensions difference between the probe and the inductor. Temperature rise can be eliminated after applying a thermoelectric cooler. It is now can be used for cell patterning.

5.2 Future Work

After quantization of magnetic field and temperature, the next step is to applying the device on cells, testifying the magnetic field effect on them.

It can be utilized on different kind of cells.

The width, spacing, turns of the inductor can be modified to reach better centralization of magnetic field. Temperature rise should be able to be avoided by improving the design.

References

- [1] Suh KY, Seong J, Khademhosseini A, Laibinis PE, Langer R. A simple soft lithographic route to fabrication of poly(ethyleneglycol) microstructures for protein and cell patterning. *Biomaterials* 2004;25:557-563.
- [2] Kane RS, Takayama S, Ostuni E, Ingber DE, Whitesides GM. Patterning proteins and cells using soft lithography. *Biomaterials* 1999;20:2363-2376.
- [3] Odde DJ, Renn MJ. Laser-Guided Direct Writing of Living Cells. *Biotechnology and bioengineering* 2000;67:312-318.
- [4] Roth EA, Xu T, Das M, gregory C, Hickman JJ, Boland T. Inkjet printing for high-throughput cell patterning. *Biomaterials* 2004;25:3707-3715.
- [5] Nikolovski J, Mooney DJ. Smooth muscle cell adhesion to tissue engineering scaffolds. *Biomaterials* 2000;21:2025-2032.
- [6] Hutmacher DW. Scaffolds in tissue engineering bone and cartilage. *Biomaterials* 2000;21:2529-2543.
- [7] Kogler WS, Griffith LG. Osteoblast response to PLGA tissue engineering scaffolds with PEO modified surface chemistries and demonstration of patterned cell response. *Biomaterials* 2004;25:2819-2830.
- [8] Vunjak-Novakovic G, Obradovic B, Martin I, Bursac PM, Langer R, Freed LE. Dynamic Cell Seeding of Polymer Scaffolds for Cartilage Tissue Engineering. *Biotechnology Progress* 1998;14:193-202.
- [9] Grande DA, Halberstadt C, Naughton G, Schwartz R, Manji R. Evaluation of matrix scaffolds for tissue engineering of articular cartilage grafts. *Journal of Biomedical Materials Research* 1997;34:211-220.
- [10] Yang J, Shi GX, Bei JZ, Wang SG, Cao YL, Shang QX, Yang GH, Wang WJ. Fabrication and surface modification of macroporous poly(L-lactic acid) and poly(L-lactic-co-glycolic acid) (70/30) cell scaffolds for human skin fibroblast cell culture. *Journal of Biomedical Materials Research* 2002;62:438-446.
- [11] Xu CY, Inai R, Kotaki M, Ramakrishna S. Aligned biodegradable nanofibrous structure: a potential scaffold for blood vessel engineering. *Biomaterials* 2004;25:877-886.
- [12] Cheng XH, Wang YB, Hanein Y, Bohringer KF, Ratner BD. **Novel** cell patterning using microheater-controlled thermoresponsive plasma films. *JOURNAL OF BIOMEDICAL MATERIALS RESEARCH PART A* 2004;70A:159-168.
- [13] Yang M, Lim CC, Liao R, Zhang X. ORIENTED AND VECTORIAL PATTERNING OF CARDIAC MYOCYTES USING A MICROFLUIDIC DIELECTROPHORESIS CHIP - TOWARDS ENGINEERED CARDIAC TISSUE WITH CONTROLLED MACROSCOPIC ANISOTROPY. *Journal of microelectromechanical systems* 2006;15:1483-1486.
- [14] Heredia-Rojas JA, Rodriguez-De la Fuente. Cytological Effects of 60Hz Magnetic fields on Human Lymphocytes In Vitro:Sister-Chromatid Exchanges, Cell Kinetics and Mitotic Rate. *Bioelectromagnetics* 2001;22:145-149.

- [15] Katsir G, Baram SC, Parola AH. Effect of Sinusoidally Varying Magnetic Fields on Cell Proliferation and Adenosine Deaminase Specific Activity. *Bioelectromagnetics* 1998;19:46-52.
- [16] De Mattei M, Caruso A, Traina GC, Pezzetti F, Baroni T, Sollazzo V. Correlation between pulsed electromagnetic fields exposure time and cell proliferation increase in human osteosarcoma cell lines and human normal osteoblast cells *in vitro*. *Bioelectromagnetics* 1999;20:177-182.
- [17] Kwee S, Raskmark P. Changes in cell proliferation due to environmental non-ionizing radiation 1. ELF electromagnetic fields. *Bioelectrochemistry and Bioenergetics* 1995;36:109-114.
- [18] Lin H, Opler M, Head M, Blank M, Goodman R. Electromagnetic field exposure induces rapid, transitory heat shock factor activation in human cells. *JOURNAL OF CELLULAR BIOCHEMISTRY* 1997;66:482-488.
- [19] Lai H, Singh NP. Acute Exposure to a 60 Hz Magnetic Field Increases DNA Strand Breaks in Rat Brain Cells. *Bioelectromagnetics* 1997;18:156-165.
- [20] Wei M, Guizzetti M, Yost M, Costa LG. Exposure to 60-Hz Magnetic Fields and Proliferation of Human Astrocytoma Cells *in Vitro*. *Toxicology and Applied Pharmacology* 2000;162:166-176.
- [21] Wolf FI, Torsello A, Tedesco B, Fasanella S, Boninsegna A, D'Ascenzo M, Grassi C, Azzena GB, Cittadini A. 50-Hz extremely low frequency electromagnetic fields enhance cell proliferation and DNA damage: possible involvement of a redox mechanism. *Biochimica et Biophysica Acta* 2005;1743:120-129.
- [22] Ibrahim NM, Kuhn WB. An approach for the calculation of magnetic field within square spiral inductors at low frequency. *INTERNATIONAL JOURNAL OF NUMERICAL MODELLING: ELECTRONIC NETWORKS, DEVICES AND FIELDS* 2002;15:339-354.
- [23] Lin LW, Pisano AP, Carey VP. Thermal Bubble Formation on Polysilicon Micro Resistors. *Journal of Heat Transfer* 1998;120:735-742.

Vita

姓名：黃睿婉（Jui-wan Huang）

出生日期：1982 年 10 月 21 日

出生地：高雄市

E-mail：jwhuang.ee94g@nctu.edu.tw

學歷：

高雄市立高雄女子高級中學（1998.9~2001.6）

（Kaohsiung Municipal Girls' Senior High School）

國立交通大學電子工程學系（2001.9~2005.6）

（Department of Electronics Engineering, National Chiao Tung University）

國立交通大學電子研究所碩士班（2005.9~2007.7）

（Institute of Electronics, National Chiao Tung University）